ChemCatChem
Research Article
doi.org/10.1002/cctc.202500855
Chemistry Europe
European Chemical Societies Publishing
www.chemcatchem.org

Dry Reforming of Methane Over Ceria Supported Catalysts Produced by Direct Impregnation with Leachate Solution from Spent Diesel Auto-Catalysts

Alessio Varotto,[a, b] Umberto Pasqual Laverdura,*[a] Silvano Del Gobbo,[a] Nicola Lisi,[a] Francesco Bozza,[a] Laura Silvestri,[a] Anastasia Maria Moschovi,[c] Iakovos Yakoumis,[c] Zara Cherkezova-Zheleva,[d] Marta Feroci,[b] and Maria Luisa Grilli*[a]

Pt-based catalysts were fabricated by impregnating both commercial and synthesized cerium oxide powders with platinum precursors from a leachate solution coming from hydrometallurgical processing of spent diesel oxidation catalysts. Catalysts were characterized by different techniques to evaluate the amount of Pt and other impurities, the reducibility, and other physico-chemical characteristics. The effect of platinum on the crystalline structure of catalysts was investigated using Williamson-Hall and size-strain methods. H_2 temperature programmed reduction revealed a synergistic effect between platinum and CeO_2. Dry reforming of methane tests were carried out in a fixed bed reactor at gas feed ratio of $CO_2/CH_4/N_2 = 40:40:120$. The removal of residual NaCl from the leachate solution led to improved catalytic performances: catalysts prepared using commercial and synthesized CeO_2 supports showed high conversions of CH_4 and CO_2, reaching values of ~94% and ~96%, respectively, and a H_2/CO ratio up to 0.9 at 850 °C. Catalysts were also tested toward the reverse water gas shift reaction, reaching CO_2 conversion values of 60%–70%, with nearly 100% selectivity to CO. The best-performing catalyst was tested in a time-on-stream experiment designed to stress the catalysts, and, as a result, negligible amount of carbon was detected and stable conversions over time were achieved.

1. Introduction

Due to the increase of greenhouse gases (GHGs) in the atmosphere, especially methane and carbon dioxide from anthropogenic activities, climate change has become a serious concern worldwide. Capture of CO_2 and sequestration (CCS), together with its utilization (CCU), are considered among the effective approaches for mitigating climate issues,[1–5] contributing to the reduction of GHG emissions, as requested by "Fit for 55" regulations which aim at the reduction of GHGs by at least 55% by 2030.[6]

Several reactions can convert greenhouse gases into valuable products, such as methane reforming reactions, i.e., three reactions in which methane reacts with oxygen, water, or carbon dioxide. The last, the dry reforming of methane (DRM) reaction, is a valuable process able to convert at the same time the two GHGs CO_2 and CH_4 to syngas, a mixture of H_2 and CO, which can be used in the Fischer-Tropsch process to produce hydrocarbons and oxygenated chemicals.[7–11] The DRM reaction is represented in Equation (1):

$$CH_4 + CO_2 \rightleftharpoons 2H_2 + 2CO \qquad \Delta H^0_{298K} = +247\,\frac{kJ}{mol} \tag{1}$$

This reaction is highly endothermic, and it requires high temperatures, typically above 650 °C, to be promoted, due to the energy required for the breakage of C—H bonds and C═O bonds in methane (750 kJ/mol) and carbon dioxide (476 kJ/mol), respectively, as evidenced by Gibbs' equation (Equation 2):

$$\Delta G^0_f = (247 - 0,26 \times T)\ \ kJ/mol \tag{2}$$

Despite DRM reaction having a theoretical H_2/CO ratio equal to unity, this ratio is always lower due to the occurrence of the reverse water gas shift (RWGS) reaction (Equation 3), a side reaction that consumes part of H_2 and CO_2 to obtain CO and water:

$$CO_2 + H_2 \rightleftharpoons CO + H_2O \qquad \Delta H^0_{298K} = +41\,\frac{kJ}{mol} \tag{3}$$

---

[a] A. Varotto, U. Pasqual Laverdura, S. Del Gobbo, N. Lisi, F. Bozza, L. Silvestri, M. L. Grilli
Italian National Agency for New Technologies, Energy and Sustainable Economic Development (ENEA), Via Anguillarese, 301, Rome 00123, Italy
E-mail: umberto.pasqual@enea.it
mariialuisa.grilli@enea.it

[b] A. Varotto, M. Feroci
Fundamental and Applied Sciences for Engineering (SBAI), Sapienza University of Rome, Via Castro Laurenziano, 7, Rome 00161, Italy

[c] A. M. Moschovi, I. Yakoumis
MONOLITHOS Catalysts and Recycling Ltd., Vrilissou 83, Athens 114 76, Greece

[d] Z. Cherkezova-Zheleva
Institute of Catalysis, Bulgarian Academy of Sciences, Acad. G. Bonchev St., Bldg. 11, Sofia 1113, Bulgaria

Supporting information for this article is available on the WWW under https://doi.org/10.1002/cctc.202500855

This side reaction occurs at the same temperature as the DRM reaction and in the presence of a catalyst. DRM reaction is not yet scaled industrially due to several drawbacks, such as catalyst metal sintering issues due to high reaction temperature, carbon deposition due to methane decomposition, and CO disproportion reactions.[12–16] To address some of these issues, platinum is often utilized as an active catalyst, as it is known that it exhibits high catalytic activity and stability. Pt belongs to the Platinum Group Metals (PGM), which is a group of transition metals of 4d and 5d shells in the periodic table of elements, including also palladium, rhodium, ruthenium, iridium, and osmium. Despite PGMs being listed as critical raw materials (CRMs) for the EU, they are essential and almost irreplaceable in many catalytic applications, such as the reverse water gas shift, oxygen evolution reaction, oxygen reduction reaction, flue gas abatement, etc.[17–23] Using PGMs from secondary sources, especially those obtained directly from the leachate solution of spent auto-catalysts without further purification, is a valuable solution to close the PGM loop and mitigate the environmental and economic impacts of the mining and synthesis process of catalysts, allowing to decrease not only the need of primary raw materials but also the need for purification of the leachate solution.

This work demonstrates, for the first time, the successful use of Pt precursors from an acidic leachate solution produced by the hydrometallurgical recovery of spent diesel oxidation catalysts (DOCs) to prepare catalysts for the DRM reaction. The hydrometallurgical process used has been developed by Monolithos Catalysts & Recycling Ltd., involving the treatment of the spent DOCs in powder form using a solution of HCl–H_2O_2–NaCl to recover platinum under mild conditions (70 °C for 2 h), employing a high solid-to-liquid ratio of 70%. It should be noted that only mechanical preprocessing is required, without any additional pretreatment steps (thermal or chemical), thus further minimizing energy demands, showing great potential for industrial application.[17,24,25] The leachate solution containing platinum is obtained by the hydrometallurgical recovery protocol like that reported in Ref. [17].

CeO_2 was used as catalyst support for the developed Pt catalysts. The selection of CeO_2 was made because of its characteristics: good mechanical properties, excellent thermal stability, and sufficient oxygen storage capacity.[26–29] In addition, CeO_2 shows high chemical stability against the acidic leachate solution, while its basicity makes it an ideal support to promote the activation of methane and carbon dioxide.[30] This concept is very important since CeO_2 can promote the formation of oxygen vacancies (Equation 4—written using Kroger-Vink notation), which are Lewis bases, due to their capacity to donate lone pairs:

$$2Ce_{Ce}^{x} + O_{O}^{x} \rightarrow V_{O}^{\cdot\cdot} + 2Ce_{Ce}' + 0.5\ O_2 \qquad (4)$$

$2Ce_{Ce}^{x} + O_{O}^{x}$ represents O^{2-} and Ce^{4+} ions in their lattice sites, $V_{O}^{\cdot\cdot}$ is a neutral oxygen vacancy and $2Ce_{Ce}'$ is a Ce^{3+} at a Ce lattice site with an effective charge of −1.[31]

Finally, it is well known that Pt and CeO_2 interact with each other even at high temperatures, and the bond between Pt—O—Ce is essential for the metal dispersion on the support.[9,32–36] In this work, the interaction between Pt and Ce was investigated with H_2-TPR analysis, while the dispersion of platinum on the catalyst was inferred by H_2-TPD after reduction of the catalysts at 850 °C.

2. Materials and Method

Cetyltrimethylammonium Bromide (CTAB, Alpha Aesar), ethanol (J.T. Baker), cerium (III) nitrate hexahydrate (ACROS organics), citric acid (VWR Chemicals), NaCl (Carlo Erba), HCl (Sigma-Aldrich), H_2O_2 (Merck), Pt black powder (Sigma-Aldrich) CeO_2 (Merck), and SiC (200–450 mesh, Sigma-Aldrich) were used without further purification. Moreover, CeO_2 was also synthesized in the laboratory with the route described below.

A leachate solution obtained from the hydrometallurgical recovery of spent DOCs according to the protocol reported in Ref. [17] and a synthetic leachate solution made by dissolving commercial Pt black powders (Merck) in HCl–H_2O_2–NaCl (HCl (Sigma-Aldrich), H_2O_2 (Merck), NaCl (Carlo Erba) were used as Pt precursors.

2.1. Catalyst Synthesis

CeO_2 was synthesized using a modified sol–gel method.[37] Figure S1 presents the steps followed to synthesize each catalyst. CTAB (5 mmol) was poured into 15 mL ethanol and sonicated at room temperature until complete dissolution. A solution containing 5 mmol of $Ce(NO_3)_3$•6 H_2O and 5 mmol of citric acid in 5 mL of ethanol was added dropwise to the CTAB solution.

After complete dissolution, heating at 60 °C to remove ethanol, and drying, the solution was calcinated in air at 500 °C for 5 h in a muffle, with a heating rate of 5 °C/min, to remove organic precursors. The obtained powder was denominated CS, while the commercial cerium oxide, used for comparison, was named CC (Table S1). A wet impregnation method was used to impregnate the CeO_2 support with platinum precursors contained in the leachate solution of DOCs. The concentration of Pt metal in the leachate solution was equal to 2064 mg Pt/L. It should be noted that the leachate solution was used without any further refinement steps. Thus, the leachate solution also contained other impurities such as Al, Ca, Mg, Fe, S, Na, Cl, Ce, Zn, Cr, Ni, P, and C. These impurities can originate either from the structure of the cordierite, the reagents used for the hydrometallurgical process, or deposits of unburnt oil and carbon from the operation of the catalytic converters on the vehicle.[38–40] The required volume of platinum leachate solution was calculated based on the desired Pt loading of the catalyst (1 wt%, as confirmed by ICP-OES in Table S2) and was added to the solution containing CeO_2 in 5 mL of ethanol. The solution was dried at 60 °C until ethanol was evaporated, and then it was calcined at 500 °C for 2 h with a heating rate of 5 °C/min. The catalyst's powder after calcination was washed several times with deionized water in a centrifuge to remove NaCl residues and then calcinated again at 500 °C for 2 h at 5 °C/min. The catalyst powder obtained was denominated as CCl if the commercial cerium oxide was used and CSl if synthesized cerium oxide was used. The suffixes

-w and -nw indicate whether the catalyst's powder has been submitted to the washing procedure or not, respectively. Table S1 summarizes the nomenclature of the catalyst samples produced. To study the effect of impurities of the leachate solution, a catalyst was prepared for comparison using commercial Pt and CS as a support. Platinum black powder was dissolved in a synthetic leachate solution prepared following the same procedure used for digesting the auto-catalysts. The solution was used to impregnate the CS support, and the catalyst powder was submitted to the same calcination and washing procedure as the other catalysts to remove NaCl residues. The prepared catalyst was named CSS-w, where "CS" refers to the synthesized cerium oxide and "S" stands for synthetic.

2.2. Catalysts' Characterization

2.2.1. X-Ray Diffraction (XRD) Analysis

The structure of the supports and the catalysts has been characterized by XRD (X-ray diffraction) with a RIGAKU Smartlab X-Ray diffractometer equipped with a Cu Kα source (λ = 1.5406 Å) in the Bragg-Brentano configuration θ-θ, with 2θ = 10°–80° intervals, increments of 0.0120° and acquisition time of 0.4 s. Crystallite size was calculated using the Scherrer equation (Equation 5):

$$d\ \text{(nm)} = \frac{0.9\ \lambda}{\beta\ \cos\theta} \tag{5}$$

where 0.9 is the dimensionless crystallite shape factor, λ is the X-ray wavelength, β is the full-width half maximum (FWHM), and θ is the Bragg angle. The size and intrinsic strain of each powder were calculated using the Williamson-Hall plot (W-H) and Size-Strain plot (S-S) as reported in Refs. [41, 42]. The equations used to calculate the geometrical parameters, Equation (S1) and Equation (S2), listed in Table S3 are reported in the Supporting Information. To calculate the lattice parameter a (Å), Equation (6) was used:

$$a\ \text{(Å)} = \frac{\lambda}{2\sin\theta}\sqrt{h^2+k^2+l^2} \tag{6}$$

2.2.2. X-Ray Photoelectron Spectroscopy (XPS)

X-ray photoelectron spectroscopy (XPS) was used to analyze the surface composition of catalysts. XPS spectra were recorded using an upgraded VG Scientific ESCALab Mk 2, equipped with a dual anode X-ray source (Al Kα, Mg Kα) operating at 14 kV and 20 mA under high vacuum (10^{-9} mbar). Hard X-ray photoelectron spectroscopy (HAXPES) spectra were acquired using a Thermo Scientific ESCALAB QXi system, equipped with twin anode monochromatic X-ray sources (Al Kα and Ag Lα). Samples were measured by using Al Kα (1486.6 eV) and Ag Lα (2984.3 eV) as the X-ray probing radiations. High-resolution core spectra were fitted using synthetic Voigt function components, LF (a, b, c, d, e), with CasaXPS 2.3.35PR1.0 software. Peak identification was performed by referencing the C 1s peak at 285 eV. To enhance the signal, samples were prepared by pelletizing the powder into small discs using a die-cast and hydraulic press. The pellets were mounted on a stainless-steel sample holder with conductive carbon tape. Before measurement, samples were kept overnight under high vacuum (10^{-8} mbar) in the pre-chamber to allow degassing.

2.2.3. Raman Analysis

Raman spectroscopy was used to identify eventual carbon formed on the catalysts surface after the reaction. Micro-Raman spectrum of the spent catalyst powder was acquired by a Renishaw InVia Qontor Raman spectrometer equipped with 532, 633, and 785 nm lasers. To avoid CeO_2 photoluminescence, 785 nm exciting laser was used to perform the Raman measurement on the catalysts.

2.2.4. Scanning Electron Microscopy (SEM) Analysis

Scanning electron microscopy (SEM) images were acquired on the catalyst powders using an HR FE-SEM Zeiss Auriga Microscopy and an FE-SEM Zeiss 1530, both equipped with EDS Microanalysis.

2.2.5. H_2-Temperature Programmed Reduction (TPR)

H_2-TPR (temperature programmed reduction) was carried out using a flow-through automatic instrument (AutoChem 2950 HP Micromeritics), and to measure H_2 consumption, a TCD detector was used. For TPR, 100 mg of catalyst powder was used. Catalyst powder was pre-treated with a cleaning step in 5% O_2/He mixture at 500 °C to clean and prepare the surface for the reduction step, then a 5% H_2/Ar flow mixture (30 NmL/min) at 850 °C was used for the determination of H_2 consumption. This step was followed by a second reoxidation step in 5% O_2/He mixture at 30 NmL/min, and then the powder was heated to 1000 °C (heating rate of 10 °C/min) with a flow mixture of 5% H_2/Ar (30 NmL/min) to study the complete reduction of the ceria support at higher reduction temperature.

2.2.6. Thermogravimetric Analysis (TGA)

TGA (thermogravimetric analysis) was performed using a Mettler Toledo TG instrument. Samples were heated to 850 °C, starting from 25 °C, with a temperature rate of 10 °C/min flowing air at 30 mL/min. The thermal stability study of the supports and the catalysts was necessary due to the high temperatures used for the DRM reaction.

2.2.7. H_2-Temperature Programmed Desorption (TPD)

For TPD, 200 mg of catalyst powder was pretreated in a 5% O_2/He flow mixture (30 NmL/min) at 500 °C for 30 min. Afterward, the powder was reduced by flowing 5% H_2/Ar mixture at a 30 NmL/min flux and then heated to 850 °C (heating rate of 10 °C/min), maintaining the final temperature for 30 min. Then, the powder was cooled down to 50 °C in a hydrogen flow to promote the chemisorption of hydrogen and finally heated to 850 °C, obtaining the desorption of the hydrogen chemisorbed on the surface.

The Pt particle size and the active platinum dispersion were calculated using Equations (7) and (8):[41]

$$d_{Pt}^{TPD}\,(nm) = \frac{f\;W_{Pt}}{\rho_{Pt}\;\eta\;N_A\;S_f\;\;A_{Pt}} \times 10^5 \tag{7}$$

$$D_{Pt}\,(\%) = \frac{\eta\;S_f\;M_{Pt}}{W_{Pt}} \times 10^4 \tag{8}$$

where $f = 6$ is the geometrical factor for a spherical particle; W_{Pt} the wt% of Pt; $\rho_{Pt} = 21{,}5\ g/cm^3$ is the density of platinum; η is the quantity of H_2 adsorbed on Pt (mol/g); N_A is the Avogadro's number; $S_f = 2$ is the stoichiometric factor for the chemisorption of H_2 (Pt mol/ H_2 mol); $A_{Pt} = 6{,}54$ Å^2 is the surface area occupied by a platinum atom, and $M_{Pt} = 195{,}1$ g/mol is the atomic mass of Pt.

2.2.8. *Inductively Coupled Plasma Optical Emission Spectrometry (ICP-OES)*

An Agilent 5800 RV Inductively Coupled Plasma Optical Emission Spectrometer (ICP-OES) was used to infer the amount of platinum and impurities in the different powders. The system features a vertically oriented torch with axial argon flow, and it is equipped with a solid-state CCD detector having an operational range of 170–750 nm. The optical system includes an Echelle polychromator, providing a spectral resolution of <0.007 nm at 200 nm. The polychromator was thermostated at 35 °C and purged with argon. Due to the high stability of CeO_2, a strong acidic solution was necessary to digest the catalysts. A certain amount of catalysts has been dissolved in a flask using a protocol that is based on the work of Poolwong et al.[43] First, an aqua regia solution was used to digest platinum in a glass vessel at 80 °C under stirring. Then, a solution containing HNO_3 and H_2O_2 was used to digest cerium oxide.

In the end, a clear solution was obtained. Due to the different amounts of powder dissolved and different volumes of the flask, the different concentrations of reactants used are reported in Table S4.

2.2.9. *Brunauer–Emmett–Teller (BET)*

BET (Brunauer–Emmett–Teller) analysis was performed using a Micromeritics instrument (ASAP 2020 V4.03) to evaluate the values of surface area and pore morphology of supports and catalysts impregnated with platinum, in the equilibrium pressure range of $0.05 < p/p^0 < 0.5$. The pore size distribution (PSD) was obtained from the desorption branch of the isotherm using the BJH (Barrett–Joyner–Halenda) method, and the total pore volume was calculated from the maximum adsorption point at $p/p^0 = 0.99$. Before N_2 adsorption, the sample (200 mg) was degassed in He flow at 450 °C for 240 min.

2.3. DRM and RWGS Catalytic and Time-on-Stream (ToS) Tests

DRM tests were conducted in a fixed-bed reactor: a quartz tube ($d_i = 9$ mm) inserted in a tubular furnace connected to a flow apparatus at atmospheric pressure with independent mass flow regulators (Bronhorst EL-Prestige). The temperature was registered using a thermocouple in contact with the catalyst. To keep the gas hourly space velocity (GHSV) constant, about 200 mg of catalyst powder was positioned inside the reactor mixed with 1.2 g of SiC powder. The sample was pre-reduced in situ with H_2/N_2 flow 20 vol.% (200 mL/min), increasing the furnace temperature from 100 to 850 °C, at a ramp of 10 °C/min and maintaining it at 850 °C for 1 h. The reagent mixture $CH_4/CO_2/N_2 = 40{:}40{:}120$ (total flow rate of 200 mL/min) was introduced into the reactor at 450 °C. The catalytic test was performed in the temperature range of 450–850 °C.

The conversion of reactants (CH_4 and CO_2) was calculated using Equation (9) using N_2 as an internal standard:

$$X_{conv.} = 100\left(1 - \frac{C_i\,C_{N_2}^0}{C_i^0\,C_{N_2}}\right) \tag{9}$$

$C_{N_2}^0$(%) and C_i^0(%) are the inlet concentrations, and C_i(%) and C_{N_2}(%) are the outlet concentrations of the reactants (i = CH_4 or CO_2) and of N_2, respectively. H_2/CO ratio was calculated dividing the outlet concentration of H_2 by the outlet concentration of CO.

Equations (10) and (11) were used to calculate the selectivity of CO and CH_4 in the RWGS reaction:

$$Y_{CH_4}\,(\%) = 100\left(\frac{C_{CH_4}}{C_{CH_4} + C_{CO}}\right) \tag{10}$$

$$Y_{CO}\,(\%) = 100\left(\frac{C_{CO}}{C_{CO} + C_{CH_4}}\right) \tag{11}$$

$$-r_i\left(\mathrm{mol} * \mathrm{g}^{-1}\mathrm{s}^{-1}\right) = \frac{F_i * X_i}{m_{cat}} \tag{12}$$

$$\ln\,(r_i) = -\frac{E_a}{RT} + C \tag{13}$$

The reaction rate of reactants (i = CH_4 and CO_2) was calculated with Equation (12), where F_i is the inlet flow of reactants and m_{cat} is the catalyst mass.

E_a is the apparent activation energy estimated by the Arrhenius plot, based on Equation (13), where R is 8.31 JK/mol, T (K) is the reaction temperature, and C is the natural logarithm of the pre-exponential factor.

Spent catalysts after the DRM test were separated from SiC by a 325-mesh sieve. Then, the spent catalyst powders were analyzed by SEM-EDS, XRD, and Raman to explore eventual changes in the morphology, structure, or composition. Time-on-stream (ToS) catalytic tests were conducted using the same reagent mixture for DRM and RWGS reactions at 650, 750, and 850 °C, with a temperature rate of 5 °C/min and each isothermal step of 5 h.

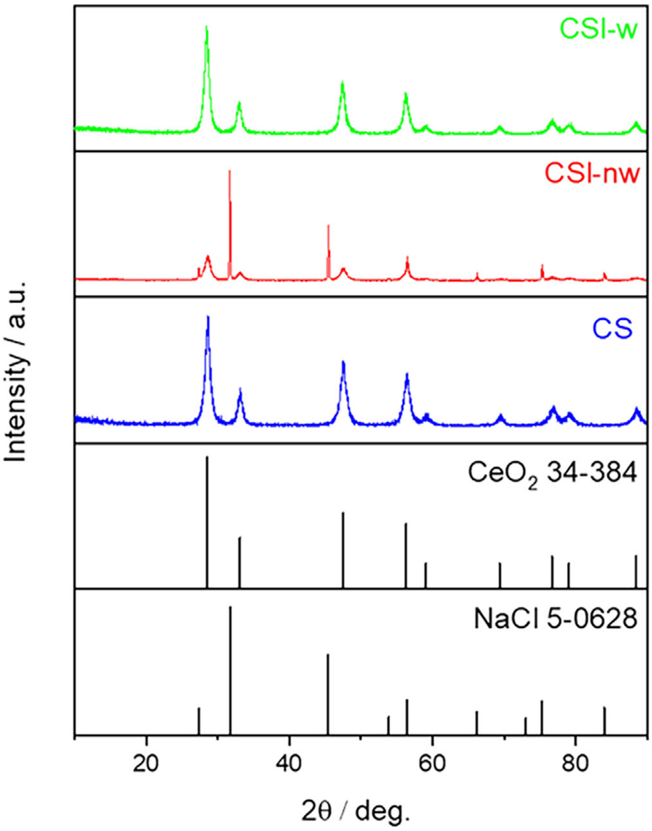

Figure 1. XRD patterns of CS support, CSI-nw and CSI-w catalysts, and CeO_2 and NaCl reference cards.

3. Results and Discussion

3.1. X-Ray Diffraction Analysis

Figure 1 reports the XRD patterns of the commercial and synthesized ceria powders and the Pt/CeO_2 catalysts. For CeO_2 supports, the characteristic diffraction peaks at $2\theta = 28.8°$ (111), 33.3° (200), 47.6° (220), 56.5° (311), 59.3° (222), 69.7° (400), 76.8° (331), 79.2° (420), and 88.5° (422) associated with the cubic face-centered phase structure of CeO_2 fluorite (JCPDS 34-384) are seen. In the case of the Pt/CeO_2 catalysts, the XRD patterns show additional peaks due to the sodium chloride phase from the leachate solution. The peaks associated with sodium chloride residues disappear after the catalyst is submitted to the washing procedure. In all the XRD spectra there is no evidence of the peak corresponding to platinum, typically at 40°, due to its low content. Figure S2 shows the XRD pattern of the spent CSI-w catalyst, from which no evident changes in the crystalline structure of CeO_2 are observed after the DRM test. However, XRD of the spent catalysts revealed peaks related to the SiC bed residues left after the sieving procedure. Figure 1 reports only the XRD patterns of catalysts supported on CS because no significant changes occur in the case of CC support (Figure S3). To study the dimensions of crystallites and strain of catalysts, two mathematical models have been used: the Williamson-Hall plot, which considers peaks as a function of 2θ and allows to infer strain broadening and crystallite size, and the size-strain plot, which has the advantage that less weight is given to data from reflections at high angles, where the precision is usually lower.[44]

The reticular parameter reported in Table 1, calculated with Scherrer's equation (Equation 5) is consistent with the expected value (5.41 Å), suggesting that the incorporation of platinum in the cerium oxide lattice with the formation of a solid solution is excluded.[41] The size-strain plot was considered to infer the average size of crystallites: the grain size of CC is about 31.5 nm, and that of CS is 10.1 nm. A different behavior was observed between catalysts prepared from commercial and synthesized cerium oxide: a slight decrease in the crystallite size (*d*) from 14.6 to 11.2 nm was observed in CSI-nw and CSI-w, while an increase from 43.3 to 60.3 nm was found from CCI-nw to CCI-w. The difference between the two trends can probably be attributed to the different interaction between Pt and the metal impurities contained in the leachate solution with the cerium oxide support, due to the different surface areas of CC and CI supports, which influence sintering.

The Williamson-Hall analysis reveals that the strain is similar for CC and CS supports, 0.003 and 0.0028, respectively, while it decreases from 0.003 to 0.0019 and 0.0008 in CCI-w and CCI-nw, respectively. The opposite behavior is observed in CSI catalysts: strain increases to 0.0038 and 0.0032 for CSI-nw and CSI-w, and the different behavior can be attributed to the difference in sintering after calcination.

In the case of powders reduced under H_2 flow (labeled with R), an increase in the strain was observed in CCI-w_R (0.0012) and CCI-nw_R (0.0036) catalysts compared to CCI-nw (0.0019) and CCI-w (0.0008). A decrease of crystallite sizes occurs, showing a rearrangement of the lattice structure due to reduction of the Pt, the ceria structure, and the other impurities (Table 1).

3.2. X-Ray Photoelectric Spectroscopy Analysis

XPS analysis was performed in the Ce 3d and Pt 4f spectral regions. Figure 2 presents the spectrum of the CSI-w sample in these regions, and in Figure S6A,B, the survey spectra of this catalyst using the two different x-ray sources (Al Kα and Ag Lα) have been reported, while XPS spectra of other samples are shown in Figures S7 and S8. The Ce 3d spectrum is split into multiple components due to the interplay of three factors: spin-orbit interaction, hybridization of the f orbital with the d orbital, and additional electronic effects.[45] The Pt 4f spectrum exhibits two symmetric components, Pt $4f_{7/2}$ and Pt $4f_{5/2}$, separated by 3.35 eV. These can be attributed to PtO and PtO_2, as indicated by the binding energy slightly above 74 eV (Pt $4f_{7/2}$) and the symmetry of the peaks. Notably, metallic Pt nanoparticles would produce Doniach-Sunjic-type asymmetric peaks.[46] In CSI-w and CCI-w samples, the Pt 4f signal partially overlaps with the two Al 2p peaks originating from aluminum in the dissolved cordierite, which serves as the Pt support in the exhaust catalyst. Nevertheless, deconvolution effectively separates these peaks. The binding energies of Ce 3d and Pt 4f components are reported in Table S5, aligning with literature values for CeO_2 and metallic Pt.[47] To further confirm the presence of Pt and obtain a quantification, the Pt 3d peak[48] was

Table 1. Geometrical parameters and particle dimensions of CC and CS supports and calcinated and reduced Pt/CeO_2 catalysts at 850 °C, calculated from X-ray diffraction peaks using two different models (plots of Williamson-Hall and size-strain are reported in Figures S4 and S5).

Sample	Scherrer Equation	Size-strain Plot			Williamson-Hall Plot		
	a (Å)	d_{CeO_2} (nm)	ε^{S-S} (10^{-3})	R^2	d_{CeO_2} (nm)	ε^{W-H} (10^{-3})	R^2
CC	5.40	31.5	8.90	0.998	36.5	3.0	0.951
CS	5.40	10.1	20.0	0.991	12.3	2.8	0.845
CCl-nw	5.40	43.3	12.7	0.931	63.3	1.9	0.811
CSl-nw	5.42	14.6	28.3	0.903	17.6	3.8	0.817
CCl-w	5.42	60.3	5.70	0.971	81.6	0.8	0.819
CSl-w	5.42	11.2	28.3	0.991	13.5	3.2	0.930
CCl-nw_R	5.42	33.0	20.0	0.893	73.0	3.6	0.933
CSl-nw_R	5.42	40.8	14.1	0.898	44.7	1.6	0.803
CCl-w_R	5.41	51.4	6.3	0.879	77.0	1.2	0.830
CSl-w_R	5.42	25.7	20.0	0.977	42.0	3.8	0.963

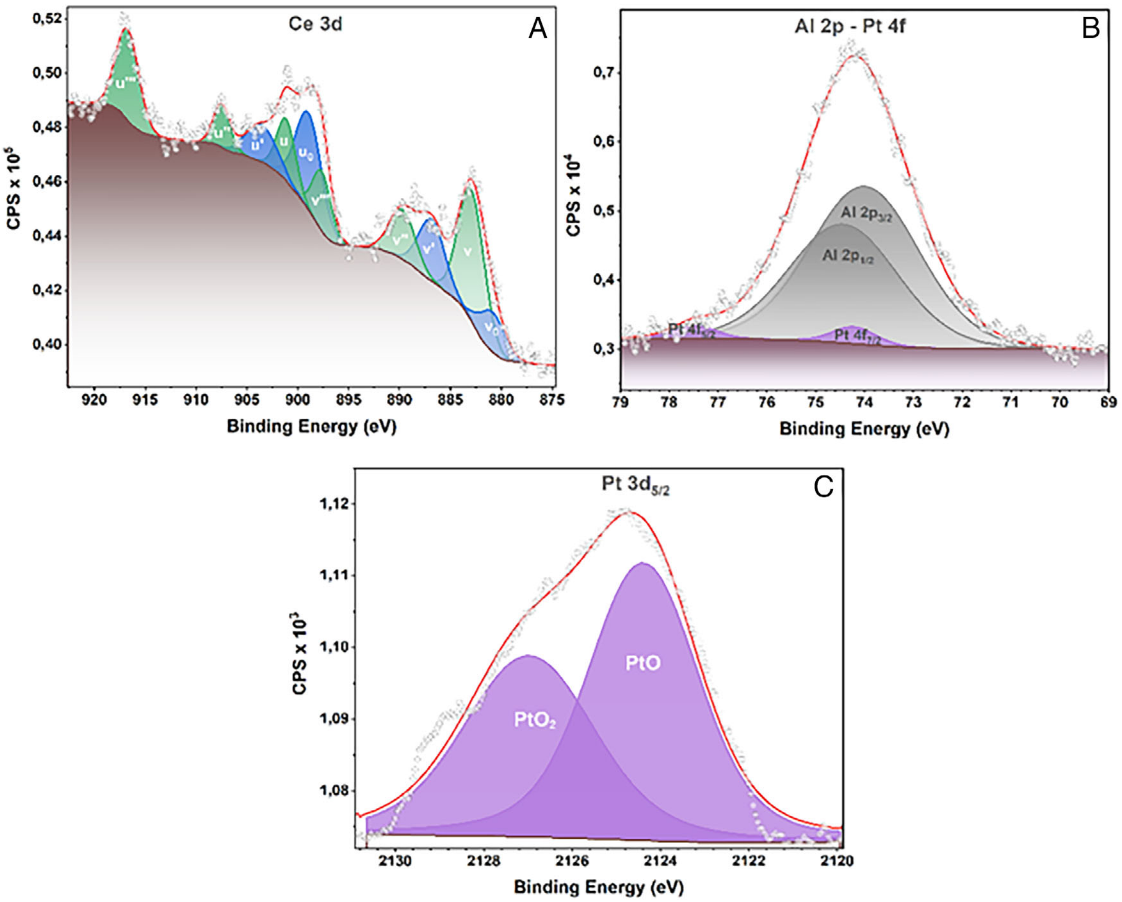

Figure 2. High-resolution XPS spectra of CSl-w sample: A) Ce 3d and Pt 4f spectral region, B) Pt 4f overlapping with Al 2p spectral region, C) HAXPES spectrum of Pt $3d_{5/2}$ spectral region.

recorded using Ag Lα as exciting X-ray radiation (2984.3 eV). The high-resolution spectrum is shown in Figure 2C. The peak was fitted by two synthetic components that can be assigned to different oxidation states of Pt[49] that we tentatively assigned to PtO and PtO_2. A comparison of the spectra across all samples shows that the Ce 3d spectra remain highly similar, with consistent numbers of components and comparable peak area intensity ratios. Following functionalization with Pt nanoparticles, the signals for both synthesized and commercial ceria remain unchanged from pristine CeO_2, as seen in Figures S7 and S8.

Quantification was performed based on the Ce 3d and Pt 4f peak areas after applying a Shirley-type background subtraction. The Ce^{3+} and Ce^{4+} content, expressed as $Ce^{3+}/(Ce^{3+} + Ce^{4+})$

and $Ce^{4+}/(Ce^{3+} + Ce^{4+})$, was determined using Equations (14) and (15). In these calculations, v^i and u^i represent the areas of the assigned synthetic components, where v^0, v', u^0, and u' correspond to Ce^{3+} final states, and v, u, v'', u'', v''', u'''; correspond to Ce^{4+} final states.[39]

$$X_{Ce^{3+}} = \frac{u_0 + v_0 + u' + v'}{\sum_i u_i + v_i} \tag{14}$$

$$X_{Ce^{4+}} = \frac{u + v + u'' + v'' + u''' + v'''}{\sum_i u_i + v_i} \tag{15}$$

Using these equations, the Ce^{3+} and Ce^{4+} atomic percentages in the CeO_2 catalyst support were estimated, with the results presented in Table S6. Both pristine commercial and synthesized ceria exhibit similar Ce^{3+}/Ce^{4+} ratios. However, after impregnation with the leachate solution, a slight decrease in Ce^{4+} concentration is observed, corresponding to a relative increase in Ce^{3+}.

As already mentioned, the Pt 4f doublet feature partially overlaps with the two Al 2p peaks, making it difficult to determine with accuracy the chemical states and content of such a small content of platinum.[49] However, by recording the Pt $3d_{5/2}$ feature using HAXPES in the high-energy range, where there is no overlap with more intense peaks from more abundant elements, it was possible to achieve a more accurate quantification of Pt. This analysis yielded a Pt/Ce atomic ratio of 3.9:96.1. Although not shown in Figure 2C, the Pt $3d_{3/2}$ feature was also detected, supporting the assignment of the peak at 2205 eV to the Pt $3d_{5/2}$ core level.

3.3. Scanning Electron Microscopy Analysis

Figure 3 reports the FE-SEM micrographs of the synthesized CeO_2 powder, from which we observed that CeO_2 powder is formed by agglomerates of irregularly shaped particles of dimensions of less than 100 nm. The SEM micrographs of CSI-w before (A) and after (B) the DRM test is also presented. As evident from the SEM images, after impregnation with the acidic leachate solution, the catalysts' morphology almost remains unchanged, and no significant differences can be observed between the as-prepared and spent catalysts.

To study the composition of the samples, an EDS analysis was also conducted on the CS support and the CSI-w catalysts before and after the DRM test (Table S7). In Figure S9, the micrographs of the analyzed area of the CSI-w before (A) and after (C) the DRM test are presented, while the elemental maps are shown in Figure S9B (before DRM test) and D (after DRM test) panels. The corresponding EDS spectra are reported in Figures S10 and S11.

3.4. Material Reducibility

To evaluate the reducibility of the samples, H_2-TPR analysis was performed on both CC and CS. As expected, the resulting profiles showed no significant differences between the two materials, as illustrated in Figure S12A. Supports show peaks at 500 and 800 °C, corresponding to reduced bulk and surface oxygen species, respectively. In the CSI-w catalyst, a new peak appears in the 250–300 °C range (Figure S12B), which can be attributed to the Pt—O—Ce bond. This bond inhibits the sintering of platinum particles because the energy bond between Pt—O—Ce is higher than the one between Pt—Pt, as evidenced by Nagai et al.[50] Similar results are observed for the CCl-w catalyst. Moreover, TCD peaks are shifted to lower temperatures due to both the weakening of the Ce oxygen bond and H_2 gas adsorption, since the spillover of platinum on CeO_2 facilitates the reduction of CeO_2.[51] In addition, the peak at higher temperatures presents multiple contributions from the several metals (Al, Mg, Fe, and Ca) present in the leachate solution of DOCs. Based on the stoichiometry in Equation (16), the total hydrogen consumption for ceria reduction at 850 °C corresponds to about 56% for CC and 52% for CS, as presented in Table 2:

$$2Ce^{4+} + H_2 \rightarrow 2Ce^{3+} + 2H^{+} \tag{16}$$

CCl-w presents a peak at around 100 °C, probably due to the formation of chlorine compounds, while CSI-w has a broader peak at ~250 °C that encompasses the reduction of Pt and chloride precursor decomposition.

3.5. Thermogravimetric Analysis

Thermogravimetric analysis was conducted on the CeO_2 samples, both bare and impregnated with Pt, and no significant weight loss was detected in every case (Figure S13). Analysis was conducted up to 850 °C, the maximum temperature of the DRM reaction considered in our study.

From the TGA curves, high thermal stability of the samples before and after the impregnation of platinum is found, with the exceptions of a negligible loss at around 100 °C, due to the evaporation of the water present, and a loss of around 6%–7% at 800–850 °C due to the decomposition of NaCl.[52]

3.6. Inductively Coupled Plasma Optical Emission Spectrometry (ICP-OES)

To quantify the amount of the different elements in the leachate solution and in the catalyst's powders, an ICP-OES analysis has been carried out. The analysis confirmed the amount of 1 wt% of platinum (the chosen Pt loading) after the washing of the catalysts and 0.6 wt% of platinum when catalysts were not submitted to the washing procedure (Table S2). The complete removal of sodium chloride was confirmed by the fact that the weight percentage of Na decreased notably almost to 0 wt% when powders were submitted to the washing procedure. The wt% of the impurity elements increased after the washing step to values comparable to those of Pt.

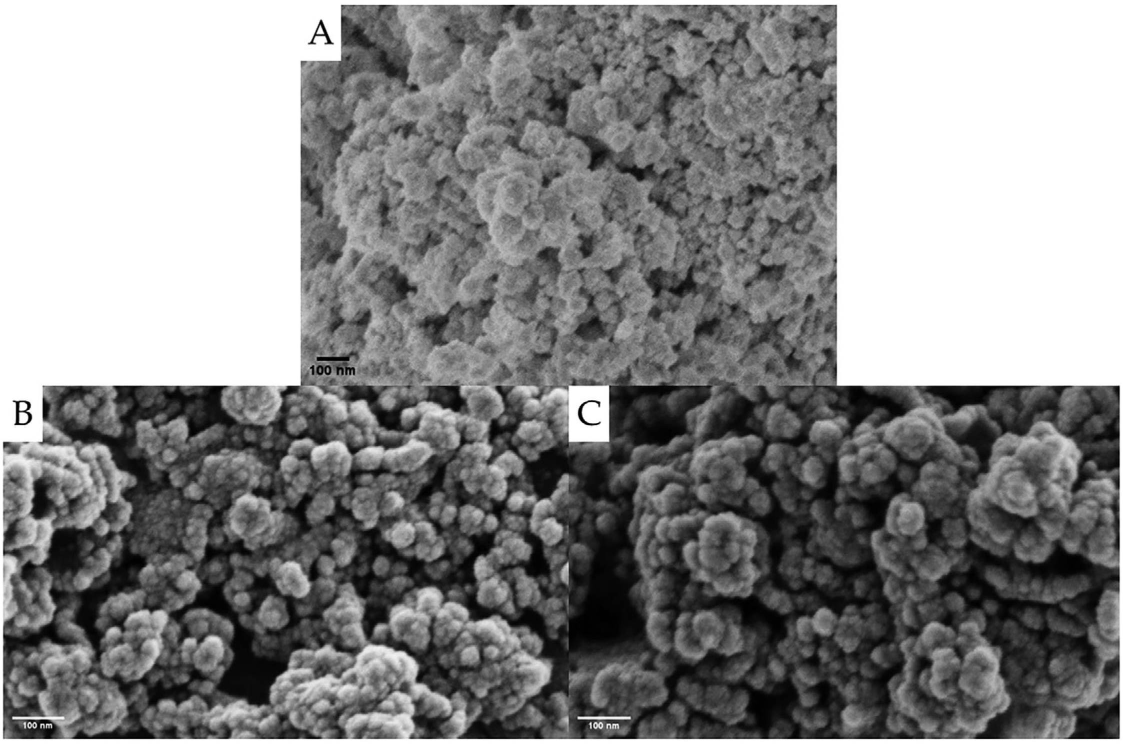

Figure 3. SEM micrograph of CS support A), CSI-w before B), and after C) the DRM test.

Table 2. PtO_2 and CeO_2 reducibility up to 850 °C.

Sample	Ce (mmol/g)	H_2 cons. (mmol/g)	H_2/Pt	H_2 cons. for Ce red.	Ce^{3+} (%)
CC	5.81	1.62	–	1.62	55.78
CS	5.81	1.52	–	1.52	52.33
CCl-w	5.69	1.55	15.12	1.52	53.40
CSl-w	5.69	2.04	19.90	2.03	71.32

3.7. Platinum Dispersion by H_2-TPD

Using H_2-TPD, analysis of platinum dispersion and particle size was investigated due to their influence on catalytic activity. As can be seen from Figure S14A, H_2 desorption in CC (black curve) and CS (red curve) starts, respectively, at 150 and 200 °C. Figure S14B reports the H_2-TPD peaks for CCl-w and CSl-w. The peaks in the range 150–200 °C show a shoulder in both cases related to the different species of H_2 that can be considered in these processes, such as spillover, adsorption of hydrogen molecules on cerium oxide support, and adsorption on platinum sites at different positions.[53–56] Miller et al.[54] studied a system with platinum supported on zeolite and obtained different H_2-TPD spectra at different reaction temperatures. In their study, H_2-TPD spectra showed the presence of more than one peak in the temperature range of 150–250 °C, in the spectra obtained with cerium oxide used as support. A strong adsorption of H_2 on the platinum surface is evident, and in both CCl-w and CSl-w the dispersion of platinum onto the support is similar (16.70% and 16.31%, respectively), as reported in Table S8.

3.8. BET Analysis

As evident from Figure 4A,B, the CeO_2 supports show N_2 adsorption–desorption isotherms classified as type II, with a type H3 hysteresis loop with parallel branches, which is typical of agglomerates.[57] Indeed, the catalysts CCl-nw, CCl-w, CSl-nw, and CSl-w show N_2 adsorption–desorption isotherms classified as type III, representing unrestricted monolayer-multilayer adsorption, which is typical for non-porous or microporous adsorbents. The hysteresis of each sample presents close loops, related to porous materials. The results of the BET analysis are reported in Table S9. The surface area of the supports (CC and CS) differs enormously due to the difference in the preparation method, as well as the use of a surfactant to increase the surface area of the synthesized powders. Surface area increases noticeably in washed catalysts with respect to the supports: from 3.4 (CC) to 83.4 (CCl-w) m^2/g and from 103.1 (CS) to 152.0 (CSl-w) m^2/g. As expected, the interaction of leachate solution and support plays an important role. The anomalous behavior observed in the case of the CSl-nw is still under investigation. In Figure 4C,D, adsorption–desorption isotherms and pore-size distribution (PSD) of CC, CCl-nw, CCl-w, CS, CSl-nw, and CSl-w are reported. The typical bell-shaped distribution is evident in the C and D panels of Figure 4.

3.9. Dry Reforming of Methane and Reverse Water Gas Shift Tests

The prepared Pt/CeO_2 catalysts were tested for DRM reaction, with the results concerning CH_4 and CO_2 conversion as a func-

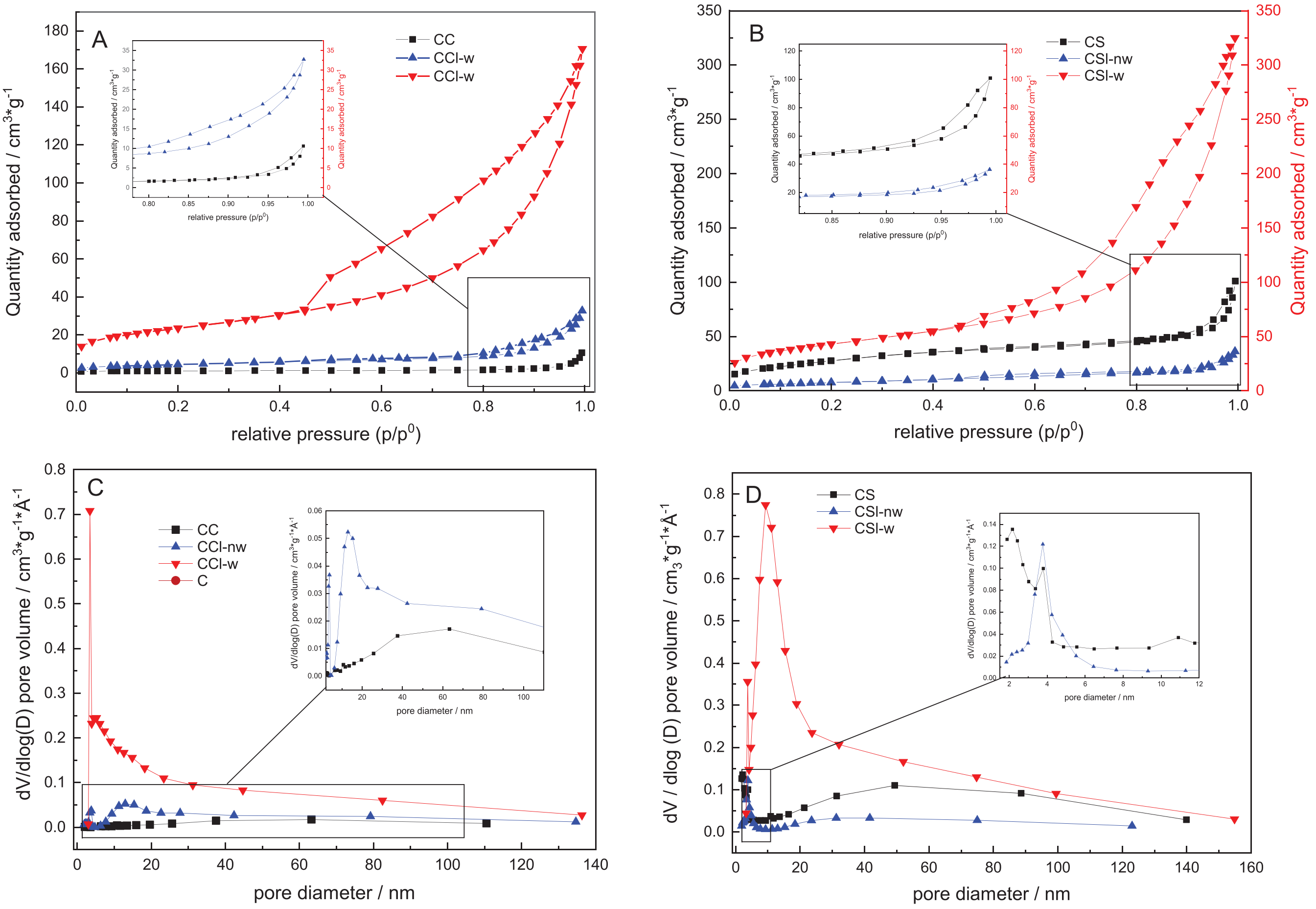

Figure 4. Adsorption–desorption isotherms of CC support (black), CCl-nw (blue), and CCl-w (red) A); CS support (black), CSI-nw (blue), and CSI-w (red); B) pore-size distribution (PSD) of CC support (black), CSI-nw (black), and CSI-w (red); and C) CS support (black), CSI-nw (black), and CSI-w (red) D).

tion of reaction temperature being reported in Figure 5A. As expected, conversions of reactants increase with temperature, since the DRM reaction is an endothermic reaction. In all cases, the conversion of CO_2 is higher than conversion of CH_4 due to the side RWGS reaction, which reduces H_2/CO ratio below 1 (Equation 3). As can be seen in Figure 5A,B, catalytic activity is increased in the case the catalysts have been submitted to the washing procedure. For the CSI-w catalysts obtained on synthesized ceria support, CH_4 and CO_2 conversions are, respectively, 94% and 96%, against the 40% and 60% of the unwashed CSI-nw catalyst. For catalysts prepared using commercial ceria as the support, much lower conversion values are obtained. For the washed catalyst (CCl-w), conversions are, in fact, 57% for CH_4 and 69% for CO_2, against the 30% and 40% for the unwashed CCl-nw catalyst. The measured H_2/CO ratios are in the range of 0.4–0.9, being lower in the case of the unwashed catalysts.

The different behavior between washed and unwashed catalysts is due to the higher wt% of platinum exposed, as confirmed by ICP-OES analysis (Table S2).

Among the catalysts synthesized using the leachate solution, CSI-w showed the best performance due to the combination of a higher percentage of Ce^{3+} related to a higher amount of oxygen vacancies (Table 2) and the higher surface area observed (Table S9). These conversion efficiencies are optimal for DRM reaction.[36,58,59]

It is worth noting that this is the first attempt to use the acidic leachate solution of spent autocatalysts directly for the preparation of catalysts for the DRM reaction, moreover, without purification. Difficulties in such an approach lie in the fact that the leachate solution not only presents a strong acidity ($pH \leq 1$) but also contains several metal impurities that may hinder the dispersion of platinum onto the cerium oxide support. The effect of such impurities has been studied by comparing the DRM performance of the CSI-w catalysts with the one of CSS-w catalyst, obtained on CS support by impregnation with the synthetic leachate solution containing only Pt as active metal (Figure S15). Both catalysts show a DRM sigmoidal curve, but the catalysts prepared with the synthetic leachate solution start flattening at about 200 °C lower temperature, reaching conversion values of reactants close to 100% at the maximum investigated temperature of 850 °C. The main difference between these two catalysts lies in the different conversion rates of methane and carbon dioxide, which is related to the value of the energy of activation. The activation energy calculated using Equations (12) and (13) for CH_4 is 10.58 kJ/mol for the CSS-w catalyst against the 15.6 kJ/mol for the CSI-w one, while for CO_2 the activation energy is 32.71 for CSI-w catalyst against the 25.97 kJ/mol for CSS-w catalyst. The dif-

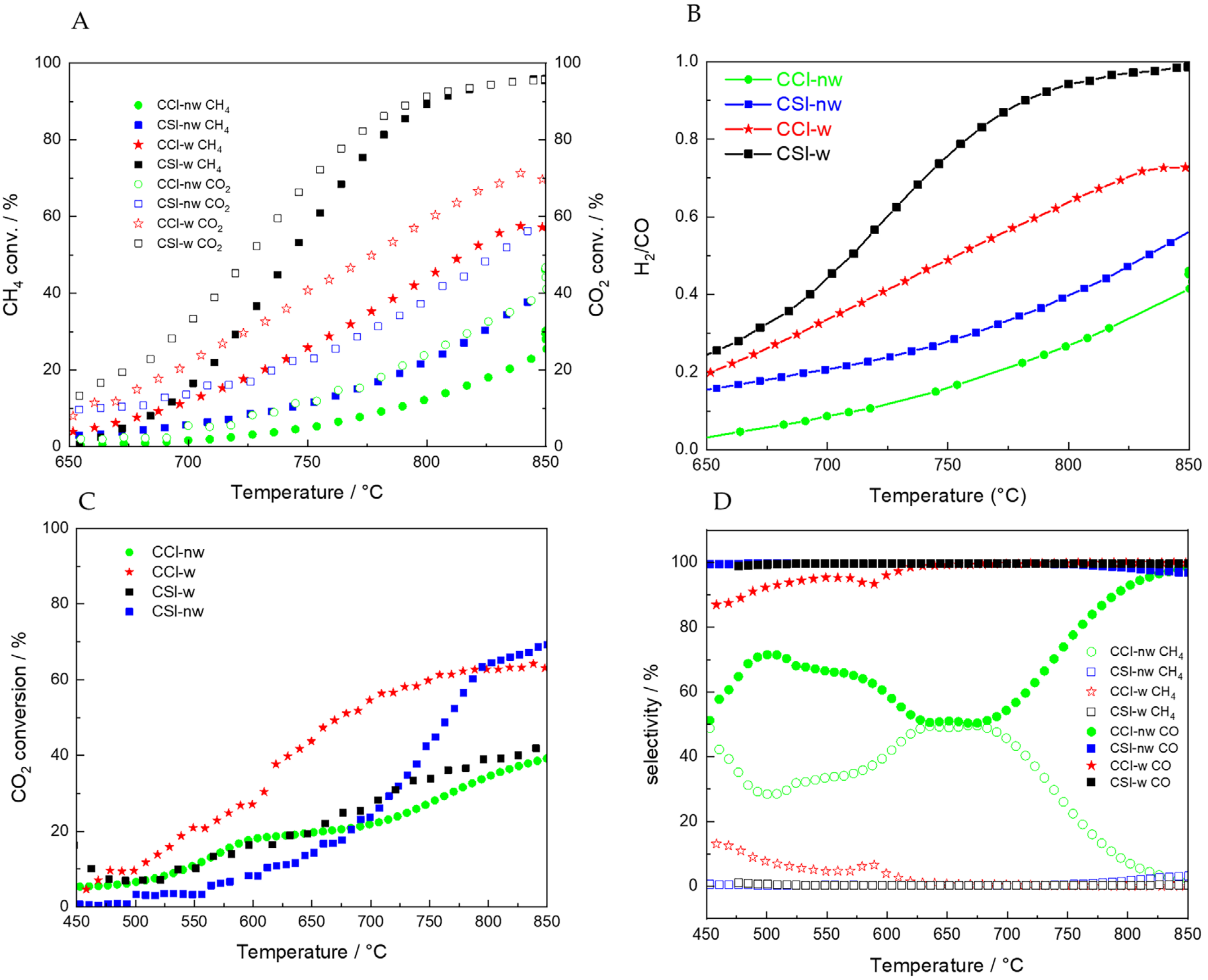

Figure 5. CH_4 and CO_2 conversions of CSI-w, CSI-nw, CCl-w, and CCl-w A) and H_2/CO ratio B) for the DRM reaction; CO_2 conversions C), CH_4 and CO selectivities D) of CSI-w, CSI-nw, CCl-w, and CCl-nw for RWGS reaction.

ference can be attributed to the effect of impurities contained in the real leachate solution, which inhibit catalyst sites on the support, thus reducing the capacity to break the C—H and C═O bonds of methane and carbon dioxide, respectively.

The catalysts' behavior toward the main competitive reaction to DRM, i.e., the RWGS reaction, was tested in a mixture of $H_2/CO_2/N_2$, using a volumetric ratio of 1:1:3 (total flux = 200 mL/min). Assessment of the catalyst's behavior for the RWGS reaction may be useful to evaluate its ability to widespread utilization of CO_2 for conversion into valuable chemicals.[60,61]

Figure 5C reports the conversions of CO_2 in the RWGS reaction. At 850 °C, conversion of carbon dioxide is in the range of 60%–70% for CCl-w, and CSI-nw catalysts. On the other hand, CCl-nw and CSI-w catalysts showed a lower conversion value of 39% at the same temperature.

Selectivities of CH_4 and CO are reported in Figure 5D. CO selectivity values close to 100% are obtained for CSI-nw, CSI-w and CCl-w in the temperature range of 625–850 °C, while for CCl-nw CO selectivity values greater than 90% are observed only at $T \geq 800$ °C. In the case of catalysts produced using the commercial CeO_2, part of carbon dioxide and hydrogen react to produce methane through the methanation reaction, which is favored at lower temperatures of 450–650 °C due to its exothermicity, but it appears that these catalysts have a much higher selectivity for carbon monoxide compared to the methane.[62–64]

For almost all the catalysts, during the RWGS tests, small amounts of methane were produced, highlighting a high selectivity toward the RWGS reaction to produce CO. This is probably due to the oxygen vacancies of cerium oxide that enhance the adsorption of CO_2 molecules, which turn into CO through the formation of intermediate carbonyl species, and the effect of surface area related to an higher amount of active sites.[65] In particular, the CCl-w catalyst showed a better performance for the RWGS reaction with a stable 60% conversion of CO_2 already at 750 °C. Also, CSI-nw and CSI-w reached a CO_2 conversion value of 60%, but at higher temperatures (> 800 °C). This temperature is significantly lower than the temperature at which the RWGS reaction is commonly carried out (900 °C to avoid the thermody-

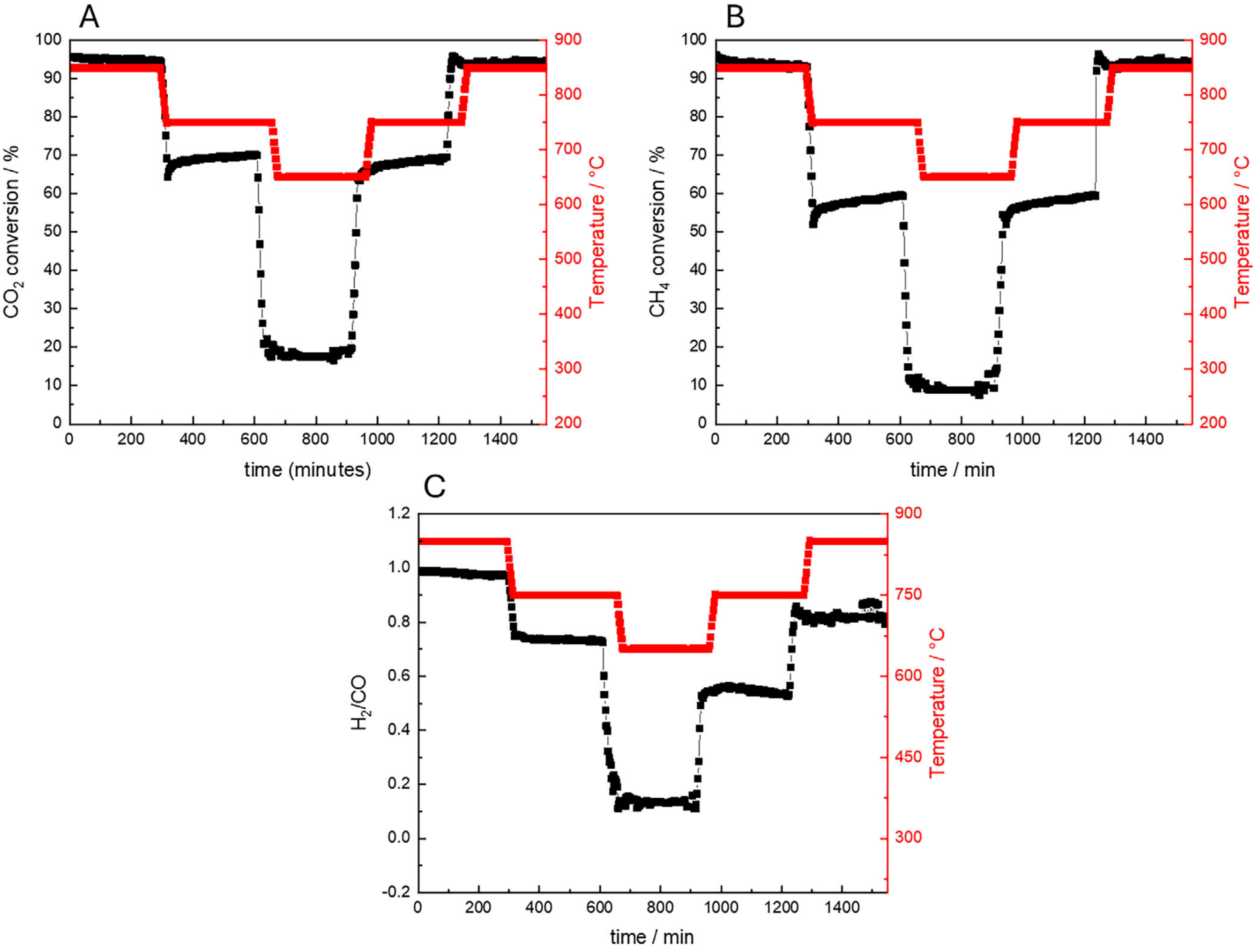

Figure 6. Time-on-stream (ToS) over CSI-w sample at 650, 750, and 850 °C, with temperature changes of 5 °C/min and each isothermal step of 5 h: CO_2 A), CH_4 B), and H_2/CO ratio C).

namic limitation of the reaction) with a conversion that is in line with other RWGS catalysts reported in the literature.[66] Therefore, the activity and selectivity of these catalysts for the RWGS opens up the possibility of employing these catalysts also for syngas production reactions from CO_2 and H_2, important for the valorization of CO_2 coming from CCS processes.[55]

To further enhance the conversions of reactants for the DRM reaction, bimetallic phase catalysts containing other PGMs besides Pt, such as Ni or Co, could be used, both aiming at decreasing the activation energies for methane and carbon dioxide,[67] and at lowering the amount of noble metals. It is worth noting, however, that the use of small amount of recycled PGMs in such applications could lead to further enhancement of the cost-effectiveness of such catalysts.

To investigate the catalysts' durability, a time-on-stream (ToS) stability test was carried out for 25 h at different temperatures on the CSI-w catalyst, the catalyst showing the better catalytic performances. The catalyst was firstly tested at 850 °C with the reaction temperature being subsequently decreased to 750 and 650 °C, prior to being raised again to 750 and 850 °C. Figure 6A,B shows the CH_4 and CO_2 conversions and the H_2/CO ratio for CSI-w during the DRM test carried out at five isothermal steps: 850, 750, and 650 °C (5 °C/min), each one lasting 5 h. Catalyst showed good stability in the first three isothermal steps, with a decrease of H_2/CO ratio to 0.8 after 9 h in the last step at 850 °C.

The stability during the test may be ascribed to the strong interaction between platinum and the support, as highlighted by H_2-TPR analysis. Moreover, stability can be enhanced by the removal of chlorine species, as already observed by Araiza et al.,[50] who employed for their catalysts H_2PtCl_6 as Pt precursors over CeO_2 support.

The durability of our catalyst confirms its high tolerance to carbon deposition, due to the oxygen storage capacity (OSC) of cerium oxide, which easily forms oxygen vacancies in a reducing environment. Raman analysis (Figure S16) also confirmed the absence of significant amounts of carbon deposited on the catalyst surface, demonstrating the ability of Pt to inhibit carbon deposition and coke during the DRM reaction.[68] The micro-Raman analysis carried out with a 785 nm exciting laser wavelength on the spent CSI-w catalyst revealed, on the several crystallites analyzed, no typical G and D bands of graphitic carbon, but only the intense F_{2g} band of CeO_2.

A ToS stability test for RWGS reaction was also carried out over the CSI-w catalyst, as shown in Figure S17. The highest value of CO_2 conversion (42%) was observed in the first isothermal step at 850 °C. A slight decrease in CO_2 conversion over time was observed.

4. Conclusions

The acidic leachate solution containing Pt precursors obtained through the hydrometallurgical recovery of diesel oxidation catalysts was used for the first time to obtain Pt-based catalysts for application in the DRM reaction. Catalysts were obtained by impregnation of commercial and synthesized ceria supports with a leachate solution containing 1 wt% Pt and other metal impurities, as measured by ICP-OES. The synthesis of CeO_2, carried out using a sol-gel method, was aimed at improving the surface area of the catalyst with the employment of CTAB surfactant solution. Performances of four different catalysts have been compared to investigate the differences due to the type of support (commercial or synthesized) and the removal of NaCl residues from the leachate solution. Results show that the washing procedure in a centrifuge was necessary to improve the performance of catalysts, resulting in a higher conversion of reactants and a higher H_2/CO ratio: the better DRM performances were obtained from the two catalysts not containing contamination of NaCl salt. The catalyst fabricated from commercial powders (CCl-w) had a conversion of 57% and 69% for methane and carbon dioxide, respectively, while the one obtained from CeO_2 synthesized in the laboratory (CSI-w) had a conversion of 94% and 96% for CH_4 and CO_2, respectively. The H_2/CO ratio at 850 °C was higher for the CSI-w catalyst, with a value of 0.9, compared to 0.7 for CCl-w catalyst. Time-on-stream analysis for DRM and RWGS reactions was performed on CSI-w at different temperatures, 850, 750, and 650 °C for 25 h, and showed good stability over time. A greater selectivity for the CO reaction was observed during the RWGS test, nearly 100% in CCl-nw, CSI-nw, and CSI-w catalysts at all the investigated temperatures. Raman analysis demonstrated the almost absence of any carbon deposition on the spent catalyst, which explains its stability over DRM and RWGS tests. The effect of impurities contained in the leachate solution, inferred by comparing the DRM performances of CSI-w catalyst with the ones of a similar catalysts containing only Pt precursors (CSS-w catalyst), was to increase the activation energy for the DRM process by probably inhibiting some Pt active sites.

Acknowledgments

Authors gratefully acknowledge the support to the activities by the following projects: (i) "Chemistry of Platinum Group Metals (CHemPGM)," H2020-MSCA-RISE-2020 101007669, (ii) Electric System Research Programme, Project 1.6 "Energy Efficiency of Industrial Products and Processes," WP 4 "Production of green H_2 from biomass gasification using efficient CO_2 capture, storage and reuse processes (PTR22-24)" and WP3 "Development of CCS for the efficiency of the HtA industry and the achievement of the Net-Zero objectives (PTR25-27)," financed by the Ministry for the Environment and Energy Security, and (iii) "Development of ECCSEL—R.I. ItaLian facilities: user access, services and loNg-Term sustainability", National Recovery And Resilience Plan (PNRR) Mission 4 "Education and research," Component 2 "From research to business," Investment 3.1.1 "Fund for the creation of an integrated system of research and innovation infrastructures."

Open access publishing facilitated by ENEA Agenzia Nazionale per Le Nuove Tecnologie l'Energia e lo Sviluppo Economico Sostenibile, as part of the Wiley - CRUI-CARE agreement.

Conflict of Interests

The authors declare no conflict of interest.

Data Availability Statement

The data that support the findings of this study are available from the corresponding author upon reasonable request.

Keywords: Dry reforming of methane · Pt/CeO_2 catalysts · Recovered platinum · Reverse water gas shift

[1] A. Abdulrasheed, A. A. Jalil, Y. Gambo, M. Ibrahim, H. U. Hambali, M. Y. Shahul Hamid, *Renewable Sustainable Energy Rev.* **2019**, *108*, 175–193.
[2] H. C. Lau, S. Ramakrishna, K. Zhang, A. V. Radhamani, *Energy Fuels* **2021**, *35*, 7364–7386.
[3] V. Becattini, P. Gabrielli, M. Mazzotti, *Ind. Eng. Chem. Res.* **2021**, *60*, 6848–6862.
[4] S. De, A. Dokania, A. Ramirez, J. Gascon, *ACS Catal.* **2020**, *10*, 14147–14185.
[5] M. M. Ramirez-Corredores, *npj Mater. Sustain.* **2024**, *2*, 1–21.
[6] Delivering the European Green Deal - European Commission, can be found under https://commission.europa.eu/strategy-and-policy/priorities-2019-2024/european-green-deal/delivering-european-green-deal_en, (accessed: August, 2025).
[7] D. Shen, Z. Li, J. Shan, G. Yu, X. Wang, Y. Zhang, C. Liu, S. Lyu, J. Li, L. Li, *Appl. Catal. B* **2022**, *318*, 121809.
[8] T. Wurzel, S. Malcus, L. Mleczko, *Chem. Eng. Sci.* **2000**, *55*, 3955–3966.
[9] N. A. K. Aramouni, J. G. Touma, B. A. Tarboush, J. Zeaiter, M. N. Ahmad, *Renewable Sustainable Energy Rev.* **2018**, *82*, 2570–2585.
[10] W. L. Luyben, *Ind. Eng. Chem. Res.* **2014**, *53*, 14423–14439.
[11] V. Havran, M. P. Duduković, C. S. Lo, *Ind. Eng. Chem. Res.* **2011**, *50*, 7089–7100.
[12] D. Pakhare, J. Spivey, *Chem. Soc. Rev.* **2014**, *43*, 7813–7837.
[13] M. C. J. Bradford, M. A. Vannice, *Catal. Rev. Sci. Eng.* **1999**, *41*, 1–42.
[14] U. Olsbye, T. Wurzel, L. Mleczko, *Ind. Eng. Chem. Res.* **1997**, *36*, 5180–5188.
[15] R. K. Parsapur, S. Chatterjee, K. W. Huang, *ACS Energy Lett.* **2020**, *5*, 2881–2885.
[16] K. Wittich, M. Krämer, N. Bottke, S. A. Schunk, *ChemCatChem* **2020**, *12*, 2130–2147.
[17] M. L. Grilli, A. E. Slobozeanu, C. Larosa, D. Paneva, I. Yakoumis, Z. Cherkezova-Zheleva, *Crystals* **2023**, *13*, 550.
[18] A. Varotto, U. Pasqual Laverdura, M. Feroci, M. L. Grilli, *Materials* **2024**, *17*, 3809.
[19] M. M. R. y Morales, A. Brunet-Manquat, H. Dib, J. L. Rousset, F. Morfin, L. Burel, D. Bourgeois, H. Kaper, *ChemCatChem* **2023**, *15*, e202300354.
[20] A. I. Stadnichenko, E. M. Slavinskaya, O. A. Stonkus, A. I. Boronin, *ChemCatChem* **2024**, *16*, e202301727.
[21] M. Khatamirad, E. Fako, S. De, M. Müller, C. Boscagli, R. Baumgarten, P. Ingale, R. N. d'Alnoncourt, F. Rosowski, S. A. Schunk, *ChemCatChem* **2023**, *15*, e202300570.
[22] J. Antony, M. Sakthivel, J. F. Drillet, *ChemCatChem* **2023**, *15*, e202201556.
[23] T. B. Ferriday, P. H. Middleton, *Int. J. Hydrogen Energy* **2021**, *46*, 18489–18510.

[24] S. Papagianni, A. M. Moschovi, E. Polyzou, I. Yakoumis, *Metals* **2021**, *12*, 31.

[25] I. Yakoumis, M. Panou, A. M. Moschovi, D. Panias, *Clean Eng. Technol.* **2021**, *3*, 100112.

[26] T. Montini, M. Melchionna, M. Monai, P. Fornasiero, *Chem. Rev.* **2016**, *116*, 5987–6041.

[27] P. Lööf, B. Kasemo, K. E. Keck, *J. Catal.* **1989**, *118*, 339–348.

[28] J. Z. Shyu, K. Otto, *J. Catal.* **1989**, *115*, 16–23.

[29] A. F. Diwell, R. R. Rajaram, H. A. Shaw, T. J. Truex, *Stud. Surf. Sci. Catal.* **1991**, *71*, 139–152.

[30] E. W. McFarland, H. Metiu, *Chem. Rev.* **2013**, *113*, 4391–4427.

[31] P. R. L. Keating, D. O. Scanlon, G. W. Watson, *Chem. Phys. Lett.* **2014**, *608*, 239–243.

[32] J. Lee, Y. Ryou, X. Chan, T. J. Kim, D. H. Kim, *J. Phys. Chem. C* **2016**, *120*, 25870–25879.

[33] L. P. Teh, H. D. Setiabudi, S. N. Timmiati, M. A. A. Aziz, N. H. R. Annuar, N. N. Ruslan, *Chem. Eng. Sci.* **2021**, *242*, 116606.

[34] F. Zhang, R. A. Gutiérrez, P. G. Lustemberg, Z. Liu, N. Rui, T. Wu, P. J. Ramírez, W. Xu, H. Idriss, M. V. Ganduglia-Pirovano, S. D. Senanayake, J. A. Rodriguez, *ACS Catal.* **2021**, *11*, 1613–1623.

[35] H. Wang, G. Cui, H. Lu, Z. Li, L. Wang, H. Meng, J. Li, H. Yan, Y. Yang, M. Wei, *Nat. Commun.* **2024**, *15*, 1–10.

[36] D. Shen, Z. Li, Y. Bai, J. Li, S. Lyu, Y. Zhang, J. Li, L. Li, *Langmuir* **2024**, *40*, 13458–13466.

[37] Z. Du, F. Pan, E. Sarnello, X. Feng, Y. Gang, T. Li, Y. Li, *J. Phys. Chem. C* **2021**, *125*, 18684–18692.

[38] T. Abo Atia, W. Wouters, G. Monforte, J. Spooren, *Resour. Conserv. Recycl.* **2021**, *166*, 105349.

[39] A. M. Moschovi, M. Giuliano, M. Kourtelesis, G. Nicol, E. Polyzou, F. Parussa, I. Yakoumis, M. F. Sgroi, *Catalysts* **2021**, *11*, 942.

[40] M. Giuliano, M. C. Valsania, P. Ticali, E. Sartoretti, S. Morandi, S. Bensaid, G. Ricchiardi, M. Sgroi, *Catalysts* **2021**, *11*, 247.

[41] S. Tuti, I. Luisetto, U. Pasqual Laverdura, E. Marconi, *Reactions* **2022**, *3*, 333–351.

[42] D. Nath, F. Singh, R. Das, *Mater. Chem. Phys.* **2020**, *239*, 122021.

[43] J. Poolwong, S. Del Gobbo, V. D'Elia, *J. Industr. Eng. Chem.* **2021**, *104*, 43–60.

[44] A. Khorsand Zak, W. H. A. Majid, M. E. Abrishami, R. Yousefi, *Solid State Sci.* **2011**, *13*, 251–256.

[45] O. Sodpiban, T. Kessaratikoon, J. Smith, G. Ren, S. Del Gobbo, S. Das, M. Chi, V. D'Elia, B. C. Gates, *ACS Appl. Mater. Interfaces* **2023**, *15*, 55885–55894.

[46] C. Dablemont, P. Lang, C. Mangeney, J. Y. Piquemal, V. Petkov, F. Herbst, G. Viau, *Langmuir* **2008**, *24*, 5832–5841.

[47] K. I. Maslakov, Y. A. Teterin, A. J. Popel, A. Y. Teterin, K. E. Ivanov, S. N. Kalmykov, V. G. Petrov, P. K. Petrov, I. Farnan, *Appl. Surf. Sci.* **2018**, *448*, 154–162.

[48] S. A. Rincón-Ortiz, J. H. Quintero-Orozco, R. Ospina, *Surface Science Spectra* **2023**, *30*, https://doi.org/10.1116/6.0002800/2906490.

[49] A. V. Kalinkin, M. Y. Smirnov, A. I. Nizovskii, V. I. Bukhtiyarov, *J. Electron. Spectros. Relat. Phenomena.* **2010**, *177*, 15–18.

[50] D. G. Araiza, F. González-Vigi, A. Gómez-Cortés, J. Arenas-Alatorre, G. Díaz, D. G. Araiza, F. González-Vigi, A. Gómez-Cortés, J. Arenas-Alatorre, G. Díaz, *J. Mex. Chem. Soc.* **2021**, *65*, 1–19.

[51] W. C. Conner, J. L. Falconer, *Chem. Rev.* **1995**, *95*, 759–788.

[52] M. Broström, S. Enestam, R. Backman, K. Mäkelä, *Fuel Process. Technol.* **2013**, *105*, 142–148.

[53] P. J. Levy, M. Primet, *Appl. Catal.* **1991**, *70*, 263–276.

[54] M. Mikhail, P. D. Costa, J. Amouroux, S. Cavadias, M. Tatoulian, S. Ognier, M. E. Gálvez, *Fuel* **2021**, *306*, 121639.

[55] H. Wang, X. Chen, S. Gao, Z. Wu, Y. Liu, X. Weng, *Catal. Sci. Technol.* **2013**, *3*, 715–722.

[56] J. T. Miller, B. L. Meyers, F. S. Modica, G. S. Lane, M. Vaarkamp, D. C. Koningsberger, *J. Catal.* **1993**, *143*, 395–408.

[57] K. S. W. Sing, D. H. Everett, R. A. W. Haul, L. Moscou, R. A. Pierotti, J. Rouquerol, T. Siemieniewska, *Pure Appl. Chem.* **1985**, *57*, 603–619.

[58] A. Jawad, *RSC Adv.* **2023**, *13*, 33129–33145.

[59] L. Duranti, U. P. Laverdura, E. Di Bartolomeo, M. L. Grilli, R. Chierchia, C. Larosa, A. Varotto, S. Tuti, S. Licoccia, I. Luisetto, *Int. J. Hydrogen Energy* **2025**, *106*, 1403–1416.

[60] D. Carta, T. Montini, M. F. Casula, M. Monai, S. Bullita, P. Fornasiero, A. Corrias, *J. Mater. Chem. A Mater.* **2017**, *5*, 20024–20034.

[61] M. Martinelli, M. K. Gnanamani, S. LeViness, G. Jacobs, W. D. Shafer, *Appl. Catal. A Gen.* **2020**, *608*, 117740.

[62] R. Zhou, N. Mahinpey, *Can. J. Chem. Eng.* **2023**, *101*, 3180–3212.

[63] W. Wang, J. Gong, *Front. Chem. Eng. China* **2011**, *5*, 2–10.

[64] J. Gao, Y. Wang, Y. Ping, D. Hu, G. Xu, F. Gu, F. Su, *RSC Adv.* **2012**, *2*, 2358–2368.

[65] X. Chen, X. Su, B. Liang, X. Yang, X. Ren, H. Duan, Y. Huang, T. Zhang, *J. Energy Chem.* **2016**, *25*, 1051–1057.

[66] J. Gandara-Loe, Q. Zhang, J. J. Villora-Picó, A. Sepúlveda-Escribano, L. Pastor-Pérez, T. Ramirez Reina, *Energy Fuels* **2022**, *36*, 6362–6373.

[67] I. V. Yentekakis, P. Panagiotopoulou, G. Artemakis, *Appl. Catal. B* **2021**, *296*, 120210.

[68] S. R. De Miguel, I. M. J. Vilella, S. P. Maina, D. S. José-Alonso, M. C. Román-Martínez, M. J. Illán-Gómez, *Appl. Catal. A Gen.* **2012**, *435–436*, 10–18.

Manuscript received: May 11, 2025
Revised manuscript received: July 14, 2025
Accepted manuscript online: July 25, 2025
Version of record online: September 9, 2025